

Evidence of geomagnetic effect on extensive air showers in the ARGO-YBJ data

P. BERNARDINI¹, G. MANCARELLA¹, L. PERRONE¹, S.N. SBANO¹, G. ZIZZI²
ON BEHALF OF THE ARGO-YBJ COLLABORATION

¹INFN and Dipartimento di Matematica e Fisica dell'Università del Salento, Lecce, Italy

²INFN-CNAF, Bologna, Italy

paolo.bernardini@le.infn.it

Abstract: The geomagnetic field causes not only the East-West effect on the primary cosmic rays but also affects the trajectories of the secondary charged particles in the showers, causing their lateral distribution to be stretched along certain directions. Thus both the density of the secondaries near the shower axis and the trigger efficiency of a detector array decrease. The effect depends on age and direction of the showers, thus introducing modulation in the measured azimuthal distribution. Here the non-uniformity of the azimuthal distribution of the showers with the core inside the ARGO-YBJ detector is investigated for different zenith angles on the light of this effect.

Keywords: Geomagnetic Field - Extensive Air Showers - ARGO-YBJ Detector

1 Introduction

The path of charged primary cosmic rays (CR) is deflected by magnetic fields. The galactic magnetic field randomizes the CR directions. The geomagnetic field (GeoMF) restrains low-rigidity CR's from reaching the terrestrial atmosphere and causes that the CR flux is lower from East than from West. The GeoMF acts also on the charged particles of the extensive air showers (EAS) during their travel in the atmosphere. Cocconi [1] suggested that the lateral displacement induced by the Earth magnetic field is not negligible with respect to the Coulomb scattering when the shower is young. According to Cocconi model the effect could increase for high altitude measurements. Moreover if the trigger efficiency of an array is sensitive to the shower lateral extension, the GeoMF can change the acquisition rate as a function of zenith and azimuth angles.

An azimuthal modulation was observed at the Yakutsk array for EAS with energy above 50 PeV [2]. The GeoMF effect in the ARGO-YBJ data has been already foreseen and observed [3]. Here those studies are updated and the GeoMF effect appears evident in a very large data sample.

2 Detector

ARGO-YBJ [4] is an array located in the YangBaJing (YBJ) village (Tibet, P.R. of China) at 4300 m above sea level (90°31'50"E, 30°06'38"N). The full-coverage active area used for trigger purpose is 74 × 78 m². Typically the collected EAS have an energy in the range 1 – 200 TeV, well beyond the rigidity cutoff at the YBJ site. Therefore the effect of the GeoMF on the primary trajectory is negligible.

In the ARGO-YBJ reference system the azimuth angle (ϕ) of EAS is defined with respect to the detector axes in the anticlockwise direction ($\phi = 0^\circ$ for showers aligned with the x -axis and moving towards the positive direction). Thus in the ARGO-YBJ reference system the azimuth angle of showers going towards the magnetic North is $\phi_B = 71.89^\circ \pm 0.02^\circ$. The geomagnetic field at YBJ is $B = 49.7 \mu T$ with zenith angle $\theta_B = 46.4^\circ$ according to the NOAA web site [5].

3 Toy model and simulation

The trajectory of the EAS charged particles is deflected by the GeoMF in the plane perpendicular to \vec{B} (hereafter named bending plane). Assuming small angular deviations and relativistic particles, the value (d) of the West-East shift on the shower front is expected to be

$$d = \frac{q}{2p} \left(\frac{h}{\cos\theta} \right)^2 B \sin\xi, \quad (1)$$

where q is the charge, p the particle momentum, h the generation height, θ the zenith angle and ξ the angle between \vec{B} and \vec{p} . This shift of the charged particle path in the bending plane is the main effect of the GeoMF action. Also a shift in the GeoMF direction (South-North) is foreseen because of the change in time of flight. Then Eq. (1) does not fully describe the GeoMF effect. At last the model should take into account that each particle in the shower has different values of p , θ , ϕ and h . In short a MonteCarlo simulation is necessary in order to foresee the geomagnetic effect as a function of the shower axis direction. Anyway Eq. (1) indicates an enlargement of the shower footprint. This implies a decrease of the particle density near the shower core, which is then balanced by an increase at larger distances, as pointed out in [2]. As a consequence a very small, direction dependent, reduction in the ARGO-YBJ trigger efficiency can be envisaged for showers with the core lying inside the carpet.

Beams of primary protons have been simulated in order to study the magnetic effect and to disentangle it from detector effects. All these effects are studied in the shower evolution. Hereafter the angular coordinates (θ , ϕ) are those of the shower axis, not those of the single particles. The CORSIKA code [6] has been used to reproduce the shower development and a GEANT3-based code [7] to simulate the detector response. The primary trajectory has been projected on a 10 × 10 m² ground area at the center of the carpet. The simulated data are studied with the same analysis chain used for the real data.

Detector acceptance - At first the detector acceptance has been studied by simulating the showers in absence of the GeoMF. Proton beams have been simulated with

same values of primary energy (1 *TeV*), zenith angle (27°), interaction height (19 *km*) and 5 different values of the azimuth angle ($\phi = 0^\circ, 45^\circ, 90^\circ, 135^\circ, 180^\circ$). The azimuthal distribution of the rate (λ) can be fitted by the function

$$\lambda = \lambda_0 \{1 + g_{2A} \cos[2(\phi - \phi_{2A})]\}, \quad (2)$$

where the indexes 2 and A refer to the second harmonic and the acceptance effect, respectively. Then the detector acceptance introduces an azimuthal modulation with maximum at 90° ($\phi_{2A} \sim 88.0^\circ$ from the fit) and periodicity 180°. The modulation amplitude ($g_{2A} \sim 0.2\%$ from the fit) will be estimated from the real data. This effect might be simply due to the detector asymmetry, furthermore we observe that the number of trigger elements (pads) per unit length is greater along the y-axis than along the x-axis.

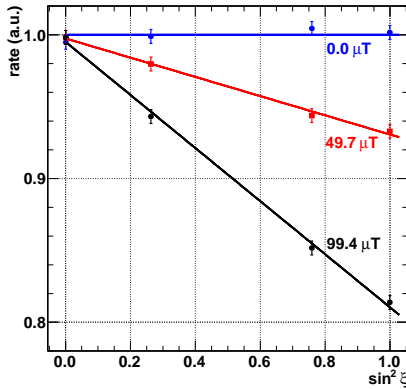


Fig. 1: Simulation: rate (arbitrary units) versus $\sin^2 \xi$ for different magnetic fields. Fit with function (3) is superimposed.

Magnetic effect - The magnetic effect has been studied by means of twelve CR beams with the same values of primary energy (3 *TeV*), zenith angle (45°) and interaction height (19 *km*). Different azimuth angles ($\phi = 71.5^\circ, 115.5^\circ, 161.5^\circ$ and 251.5°) have been used in order to get different values of the ξ angle. Also three intensities of the magnetic field have been used: 0.0, 49.7 (the actual GeoMF at the YBJ site) and 99.4 μT (twice the actual GeoMF). Looking separately at negative and positive EAS components, Eq. (1) is validated because the distance between positive and negative cores increases linearly with $\sin \xi$ and B . As expected by the toy model, when the shower axis is on the bending plane positive and negative cores are shifted precisely on the West-East axis. It has been also verified that the effect of the shower stretching on the reconstruction of the EAS direction is negligible, whereas it is significant on the trigger efficiency. Neglecting the detector effect, the rate results dependent on $\sin^2 \xi$ and the data in Fig. 1 can be fitted according to

$$\lambda = \lambda_{max} (1 - \eta \sin^2 \xi). \quad (3)$$

The term η depends linearly also on B^2 (obviously B does not vary in the real data and we will verify that η is uniform in a large range of θ). Thus we conclude that the rate reduction is proportional to $B^2 \sin^2 \xi$ and is due to the GeoMF stretching of the EAS footprint. In other words the reduction of the charge density close to the

core actually reduces the trigger efficiency when the core is on the array. The CR-beam simulation does not allow a precise estimate of the GeoMF effect but indicates the functional dependence of the trigger efficiency on B and ξ . The GeoMF effect will be fully determined by the real data analysis.

What to expect - Neglecting the detector effect, the CR-beam simulation suggests that the trigger efficiency depends on the coupling between GeoMF and EAS charged particles. From Eq. (3) we conclude that the number of events (N_θ) in an angular $\Delta\theta \times \Delta\phi$ window depends on ξ as

$$N_\theta = N_{\theta,max} (1 - \eta \sin^2 \xi), \quad (4)$$

where $N_{\theta,max}$ is the number of events expected without magnetic field and η is the previous parameter, fixed by B value, detector features and trigger conditions. A two-harmonics function is got by the calculation of $\sin^2 \xi$:

$$N_\theta = N_{\theta,0} \{1 + g_1 \cos(\phi - \phi_1) + g_2 \cos[2(\phi - \phi_2)]\}, \quad (5)$$

where

$$\phi_1 = \phi_2 = \phi_B, \quad (6)$$

$$N_{\theta,0} = N_{\theta,max} (1 - \eta A_0), \quad (7)$$

$$g_1 = \frac{\eta \sin 2\theta_B}{2(1 - \eta A_0)} \sin 2\theta, \quad (8)$$

$$g_2 = \frac{\eta \sin^2 \theta_B}{2(1 - \eta A_0)} \sin^2 \theta, \quad (9)$$

$$A_0 = \sin^2 \theta_B + \left(1 - \frac{3}{2} \sin^2 \theta_B\right) \sin^2 \theta. \quad (10)$$

From the comparison of these results with the data we will infer what is the effect of the GeoMF on the EAS development. $N_{\theta,0}$ in Eq. (7) represents the ϕ -average at fixed θ of the number of events in ϕ -bins reduced by the effect of shower stretching on the trigger.

4 Data analysis

The data set has been collected in the period October 7-14, 2010 (6.77×10^5 s). Two analysis cuts have been applied: shower core reconstructed inside a square of 40×40 *m*² at the center of the carpet, zenith angle lower than 60°. The first cut has been chosen in order to make more evident the trigger efficiency decrease (the effect is very different for showers with the core far from the detector). The second one avoids the appearance of boundary effects, moreover the analysis of data with $\theta > 60^\circ$ is not suitable because in that range the detector effect prevails on the GeoMF one. These cuts guarantee also a more reliable reconstruction of the shower direction. After cuts more than 347 millions of events have been selected (mean rate 512.8 *Hz*). Small errors in the pointing angle could introduce large systematic errors in the azimuthal distribution, especially for small zenith angles. Thus the array has been carefully time-calibrated with the characteristic plane method [8].

Rate vs $\sin^2 \xi$ - The dependence of the number of events on $\sin^2 \xi$ according to formula (4) is the first possible check. In Fig. 2 each scattered point represents the number of events in an angular window $\Delta\theta \times \Delta\phi = 2^\circ \times 5^\circ$ plotted versus $\sin^2 \xi$. The θ value is fixed for each group of points

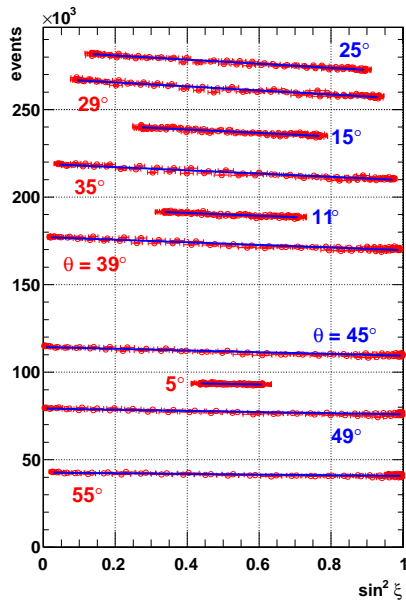


Fig. 2: Real data: scatter plot of the number of events in $\Delta\theta \times \Delta\phi = 2^\circ \times 5^\circ$ angular windows versus $\sin^2 \xi$ for different values of θ . Fits with function (4) are superimposed.

meanwhile ϕ is running. The $\sin^2 \xi$ range depends on θ , it is maximum for $\theta = 45^\circ$ and minimum for θ close to 0° . The scattered points are fitted by function (4), which is then confirmed to give a good description of the data. The η values from the fit are displayed in Fig. 3 with respect to θ . For low zenith angles the range of $\sin^2 \xi$ is so small that the fit is unreliable (the point for $\theta < 2^\circ$ is not displayed) whereas in the range $10^\circ < \theta < 50^\circ$ η is stable as expected. This method to estimate η does not separate GeoMF and detector effects and we have analytically verified that the result is an overestimate of η . For more comments about the experimental points in Fig. 3 read the final remarks in this section.

Azimuthal distribution - By integrating all showers in the range $\theta < 60^\circ$ the azimuthal distribution is shown in Fig. 4. It is well fitted by the double harmonic function (5). The phase of the first harmonic ($\phi_1 = 72.75^\circ \pm 0.29^\circ$) is compatible with the GeoMF azimuth ($\phi_B = 71.89^\circ$) as

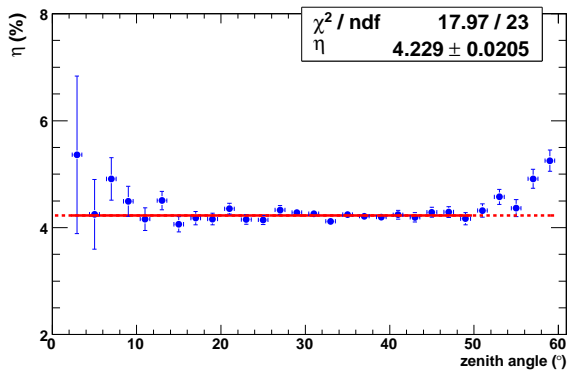


Fig. 3: Real data: the parameter η versus θ . The constant fit is performed in the θ -range $2^\circ - 50^\circ$ and extended to the whole range (dashed line).

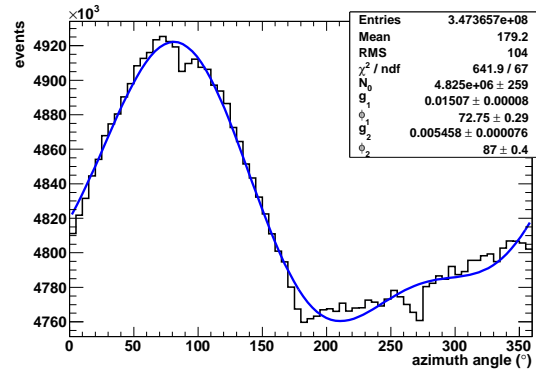


Fig. 4: Real data: azimuthal distribution and fit with function (5).

expected if the origin of the modulation is geomagnetic. This is not the case of the second harmonic phase (ϕ_2) with a value very close to what expected for the detector effect.

The high value of χ^2/ndf ($642/67 = 9.6$) is mainly due to some inefficiencies at $\phi \sim n 90^\circ$ ($n = 0, 1, 2, 3$). These dips might be due the iron beams and columns in the experimental hall. To take into account these inefficiencies, negative Gaussian curves can be added to the function. In this second fit the χ^2/ndf becomes smaller ($105/62 = 1.7$) and the parameters g_1 , ϕ_1 , g_2 and ϕ_2 do not change. The dip amplitudes are in the range $0.30 - 0.46\%$ and the Gaussian width is $\sigma = 7.45^\circ$.

Amplitude g_1 as a function of θ - The azimuthal distribution has been studied also in θ -ranges of 2° in order to check the dependence of g_1 and g_2 on θ . The result for g_1 is shown in Fig. 5 and the fit with function (8) confirms that η is constant with respect to θ . Here we like to stress that g_1 depends only on the GeoMF effect. The fractional variation of the term $(1 - \eta A_0)$ is less than 0.7% for $\theta < 60^\circ$. Then g_1 is mainly proportional to $\sin 2\theta$. According to Eq. (9) g_2 is expected mainly proportional to $\sin^2 \theta$ but the data (the plot is not shown here) have a very different shape.

Two components in the second harmonic - Meanwhile the first harmonic is in full agreement with the GeoMF model, this is not the case for the second harmonic. The tension can be solved simply taking into account that the detector effect observed in the simulation without magnetic field operates on the second harmonic. Therefore the second harmonic can be split in two parts: one (2B) is due to the GeoMF, the other one (2A) to the detector acceptance. Three different data sets have been selected on

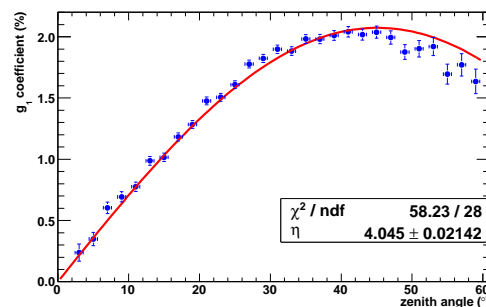


Fig. 5: Real data: coefficient g_1 versus zenith angle. The fit with function (8) is superimposed.

the basis of the zenith angle in order to disentangle these two effects. The ϕ -distributions of the subsamples (named α for $\theta < 20^\circ$, β for $20^\circ < \theta < 40^\circ$ and γ for $40^\circ < \theta < 60^\circ$) can be fitted all together with a single function:

$$N_i = N_{i,0} \left\{ 1 + \frac{\eta \sin 2\theta_B}{2(1-\eta A_0)} (\sin 2\theta)_i \cos(\phi - \phi_1) + \frac{\eta \sin^2 \theta_B}{2(1-\eta A_0)} (\sin^2 \theta)_i \cos[2(\phi - \phi_1)] + g_{2A}^i \cos[2(\phi - \phi_{2A})] \right\}, \quad (11)$$

where the coefficients of the magnetic component are deduced from Eq.s (8) and (9), the phase ϕ_1 is used for first and magnetic second harmonic and the index $i = \alpha, \beta, \gamma$ indicates the subsamples. Then the fit parameters are η , ϕ_1 , g_{2A}^α , g_{2A}^β , g_{2A}^γ and ϕ_{2A} . The new fit works very well (results in Table 1), the χ^2/ndf value is high because the dip correction has not been applied. The phase ϕ_1 and the GeoMF azimuth ϕ_B are in agreement, the η value is very close to the previous estimate. The coefficients g_{2A}^i increase with θ and ϕ_{2A} is close to 90° as expected for a detector effect.

η (%)	4.060 ± 0.019
ϕ_1 ($^\circ$)	72.22 ± 0.28
g_{2A}^α (%)	0.124 ± 0.013
g_{2A}^β (%)	0.271 ± 0.011
g_{2A}^γ (%)	1.076 ± 0.019
ϕ_{2A} ($^\circ$)	96.30 ± 0.47
χ^2/ndf	1053/210

Table 1: Results of the fit with function (11) of three azimuthal distributions (see the text for details).

Analysis final remarks - The azimuthal modulation depends on a mix of magnetic and detector effects, their contributions are shown in Fig. 6 where the coefficients g_1 , g_{2B} and g_{2A} are plotted as function of zenith angle. This plot suggests that the GeoMF origin of the rate reduction is leading with respect to the detector effect in the zenith range $20^\circ - 40^\circ$ where $g_{2A} \ll g_1$. Taking also into account that g_{2A} increases with θ the rising η values for $\theta > 50^\circ$ of the rate-vs- $\sin^2 \xi$ analysis (Fig. 3) are explained.

The measurements of the reduction coefficient η are summarized in Table 2, the first one is overestimated because of a mix of GeoMF and detector effects. The other ones are immune from the detector effect, they are lower and mutually agree. Dismissing the first measurement we conclude that $\eta = (4.053 \pm 0.014)\%$ is the proper estimate of this coefficient for the ARGO-YBJ experiment. Different values are expected for other EAS arrays because η depends on detector features, trigger requirements, geomagnetic latitude and altitude of the site.

analysis	η (%)
rate vs $\sin^2 \xi$	4.229 ± 0.021
g_1 vs θ	4.045 ± 0.021
ϕ distribution	4.060 ± 0.019

Table 2: Different estimates of the reduction factor η (same data, different analyses). The errors are only statistical.

5 Conclusions

The effect of the geomagnetic Lorentz force on EAS charged particles has been observed in a data sample collected by the ARGO-YBJ experiment. The shower extension is enlarged depending on the arrival direction with respect to the GeoMF and the different density of charged particles reduces the trigger efficiency for EAS with the core on the detector. The GeoMF origin and the features of the trigger efficiency decrease are fully understood by means of a toy model complemented by MonteCarlo simulations.

The non-uniform azimuthal distribution has been deeply studied. It is well described by two harmonics, the first one of the order of 1.5%, the second one of the order of 0.5%. The first harmonic is due to the GeoMF, the second one is the sum of magnetic and detector effects. The measurement of the geomagnetic phase ($\phi_1 = 72.22^\circ \pm 0.28^\circ$) is fully compatible with the expected value ($\phi_B = 71.89^\circ$). Other measurements confirm the geomagnetic origin of the modulation.

The phase of the first harmonic (ϕ_1) can be used as a marker of the absolute pointing accuracy of EAS arrays.

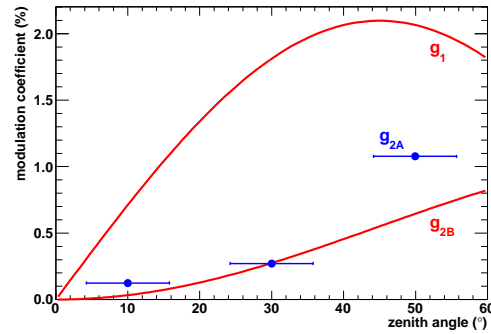


Fig. 6: Real data: coefficients g_1 , g_{2A} and g_{2B} versus θ from formulas (8), (9) and Table 1.

References

- [1] G. Cocconi, Physical Review 93 (1954) 646-647; erratum, Physical Review 95 (1954) 1705-1796.
- [2] A.A. Ivanov *et al.*, JETP Letters 69 (1999) 288-293.
- [3] H.H. He *et al.*, Proceedings of 29th Internat. Cosmic Ray Conference (Pune, 2005); P. Bernardini *et al.*, Proceedings of 32nd Internat. Cosmic Ray Conference (Beijing, 2011) 0755 (also arXiv:1110.0670); P. Bernardini *et al.*, Journal of Physics: Conference Series 409 (2013) 012229.
- [4] G. Aielli *et al.* (ARGO-YBJ Collaboration), Nuclear Instruments & Methods A 661 (2012) S50-S55.
- [5] www.ngdc.noaa.gov
- [6] www-ik.fzk.de/corsika/
- [7] GEANT - Detector Description and Simulation Tool, CERN Program Library, Long Writeup, W5013 (1993).
- [8] H.H. He *et al.*, Astroparticle Physics 27 (2007) 528-532; G. Aielli *et al.* (ARGO-YBJ Collaboration), Astroparticle Physics 30 (2009) 287-292.